Supporting Information for "Temperature dependence of frictional healing of Westerly granite: experimental observations and numerical simulations"

Erica Mitchell[1], **Yuri Fialko**[1], **Kevin Brown**[1]

[1]Institute of Geophysics and Planetary Physics, Scripps Institution of Oceanography, University of California San Diego, La Jolla, CA 92093, USA.

Contents

1. Figures S1 to S15

Introduction

This document contains supplementary figures referenced in the main text: Mitchell, E., Y. Fialko, and K. Brown, Temperature dependence of frictional healing of Westerly granite: experimental observations and numerical simulations, G-cubed, 14, 567-582, 2013.

Corresponding author: Yuri Fialko, yfialko@ucsd.edu

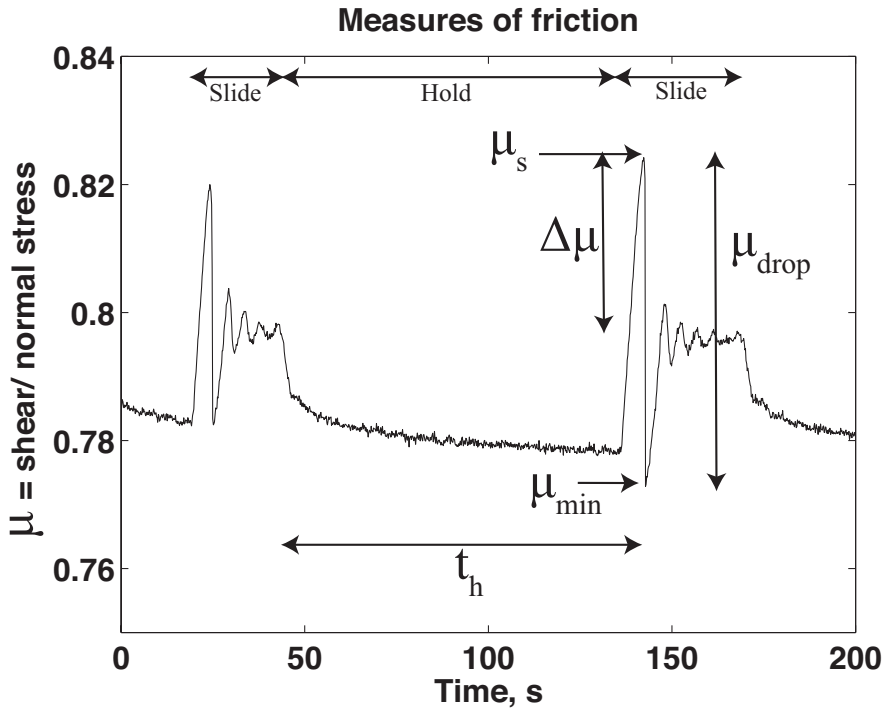

Figure S1. Typical slide-hold-slide test showing definitions of measures of t_h, μ_s, $\Delta\mu$, μ_{min}, and μ_{drop}

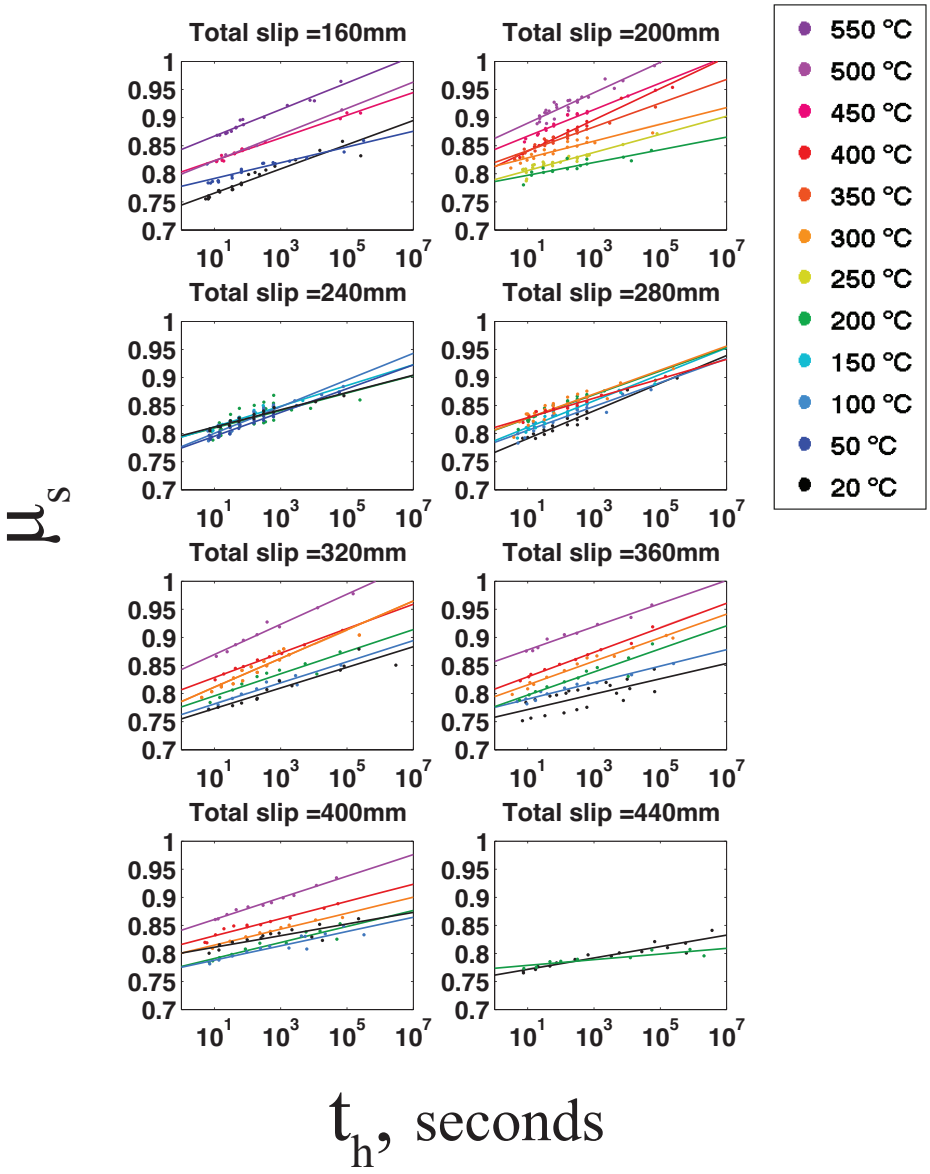

Figure S2. Static coefficient of friction vs. hold time. Color represents temperature. Each plot consists of tests done in sequence without re-setting the sample. The titles display the total slip accumulated of each plot.

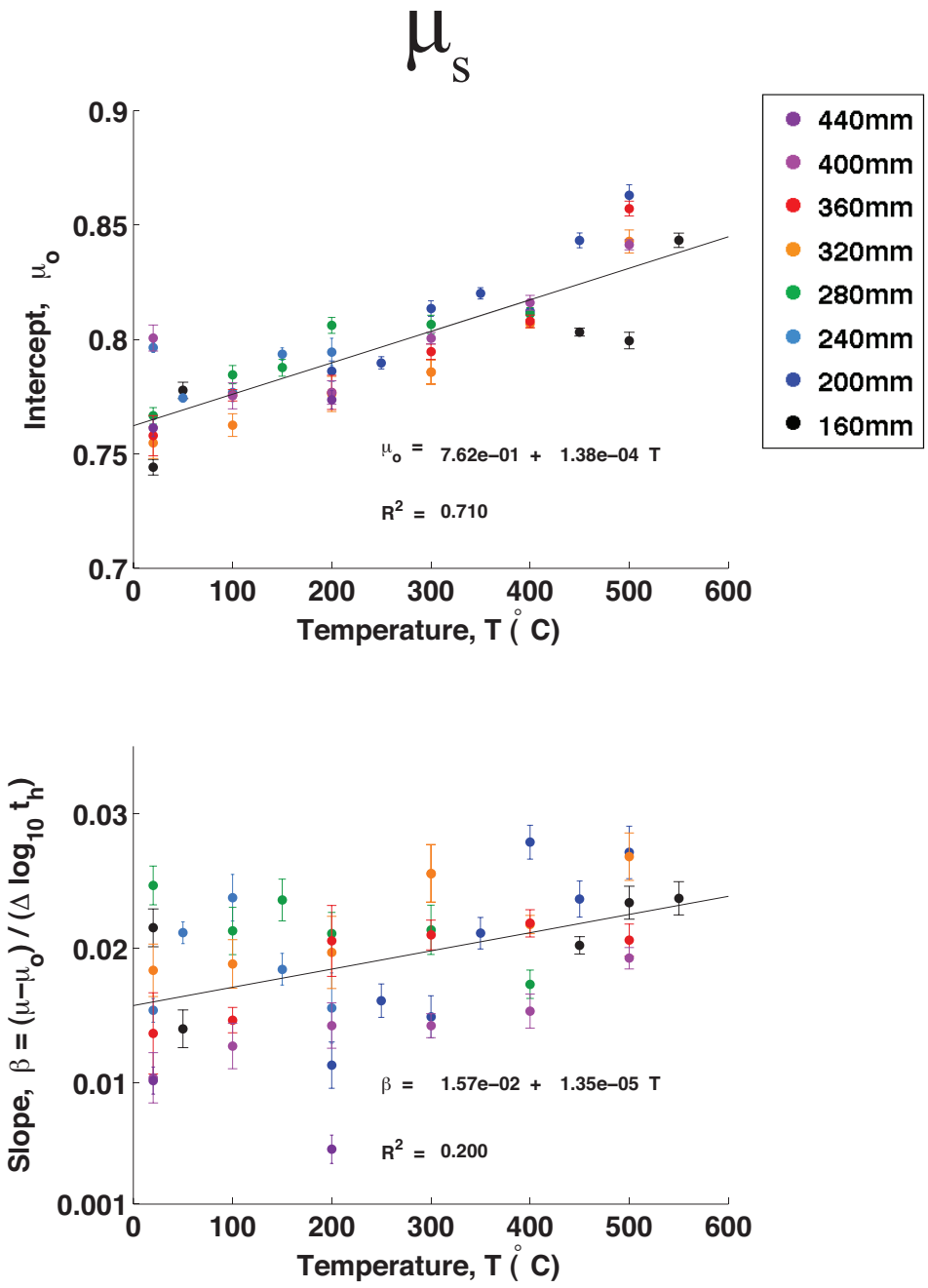

Figure S3. Slopes and intercepts fit to the static coefficient of friction data vs. temperature. Color represents total slip accumulated by the end of that series of tests.

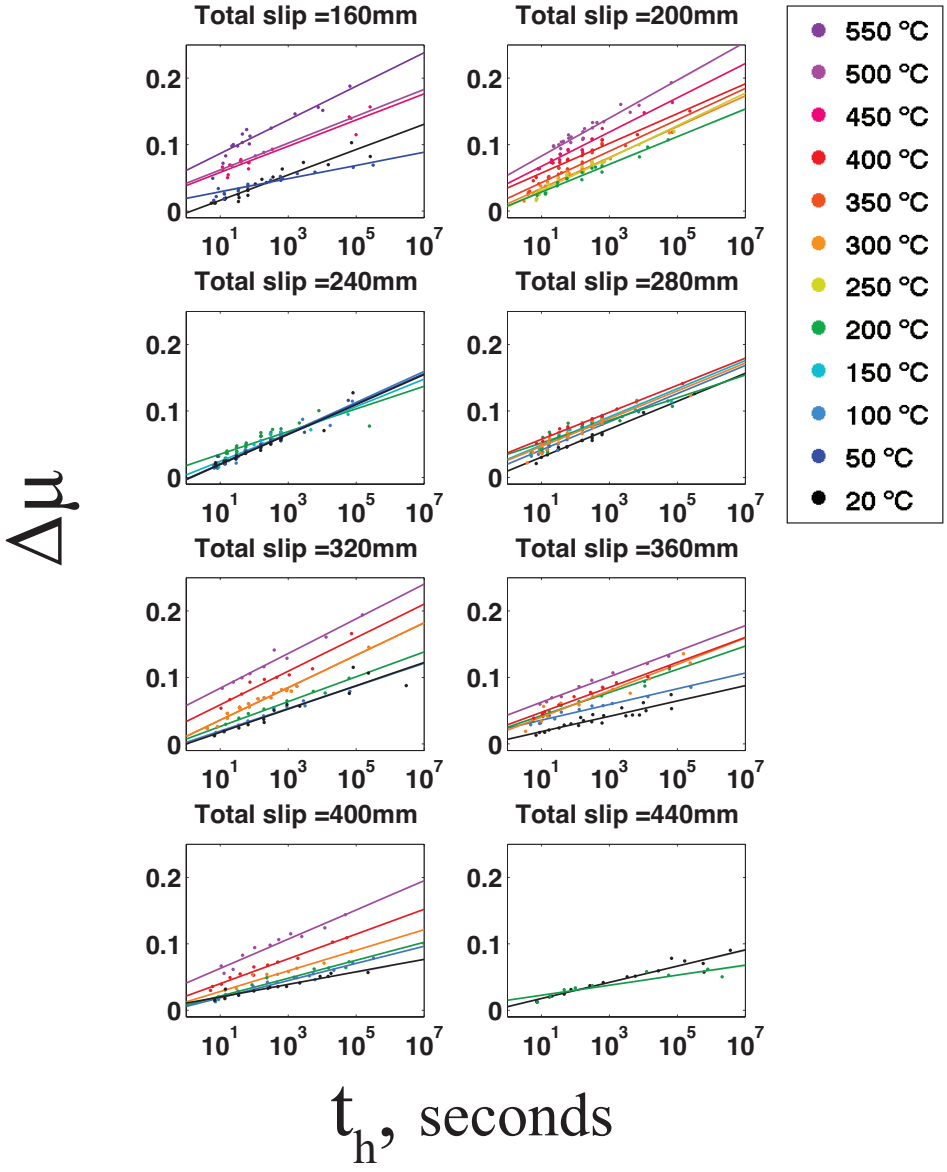

Figure S4. Increase in coefficient of friction from the steady state value (in case of stable sliding), or minimum value (in case of stick-slip) right before the hold period, to the static coefficient of friction (right before rapid slip) vs. hold time.

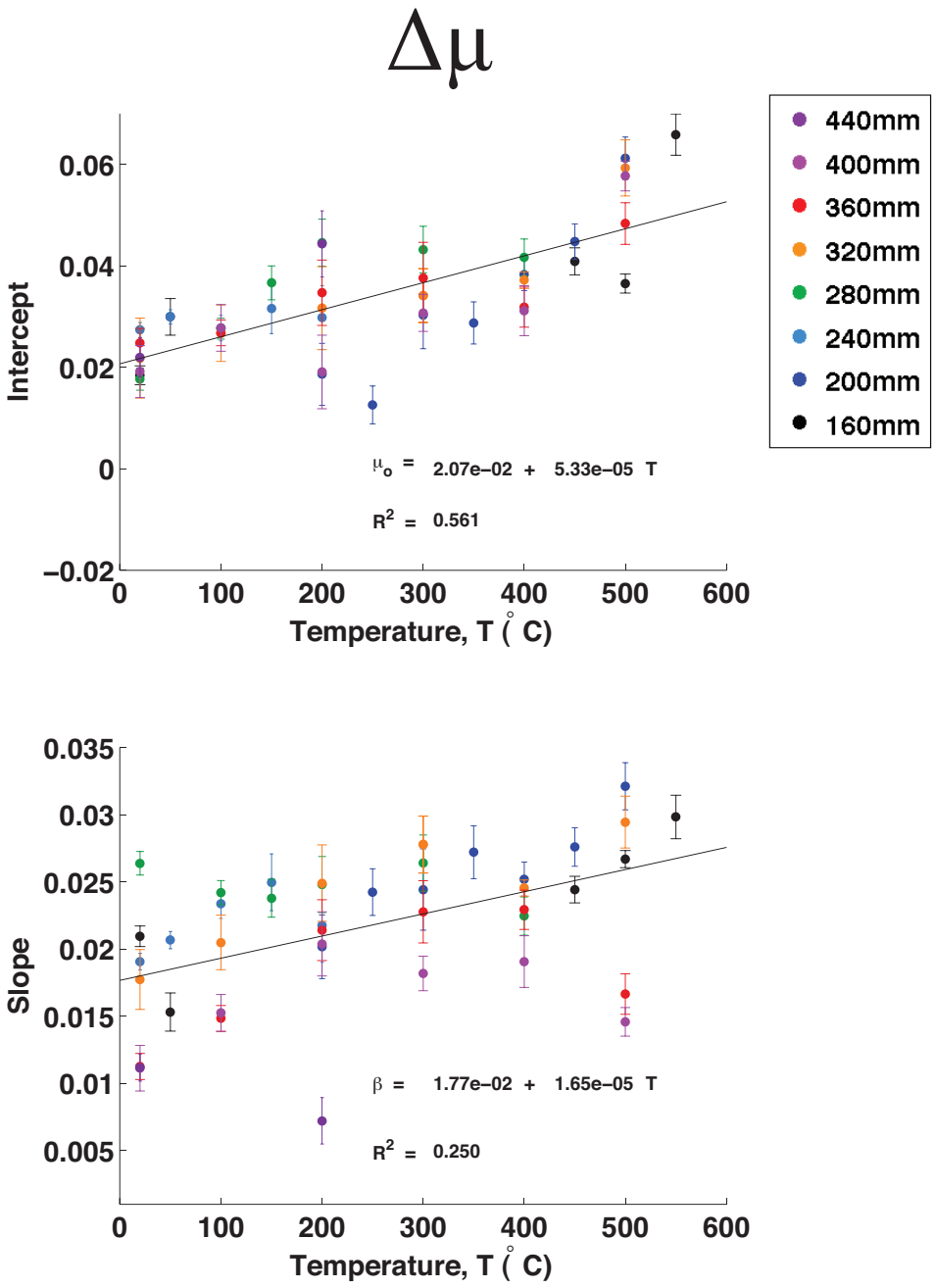

Figure S5. Slopes and intercepts fit to the $\Delta\mu$ data vs. temperature.

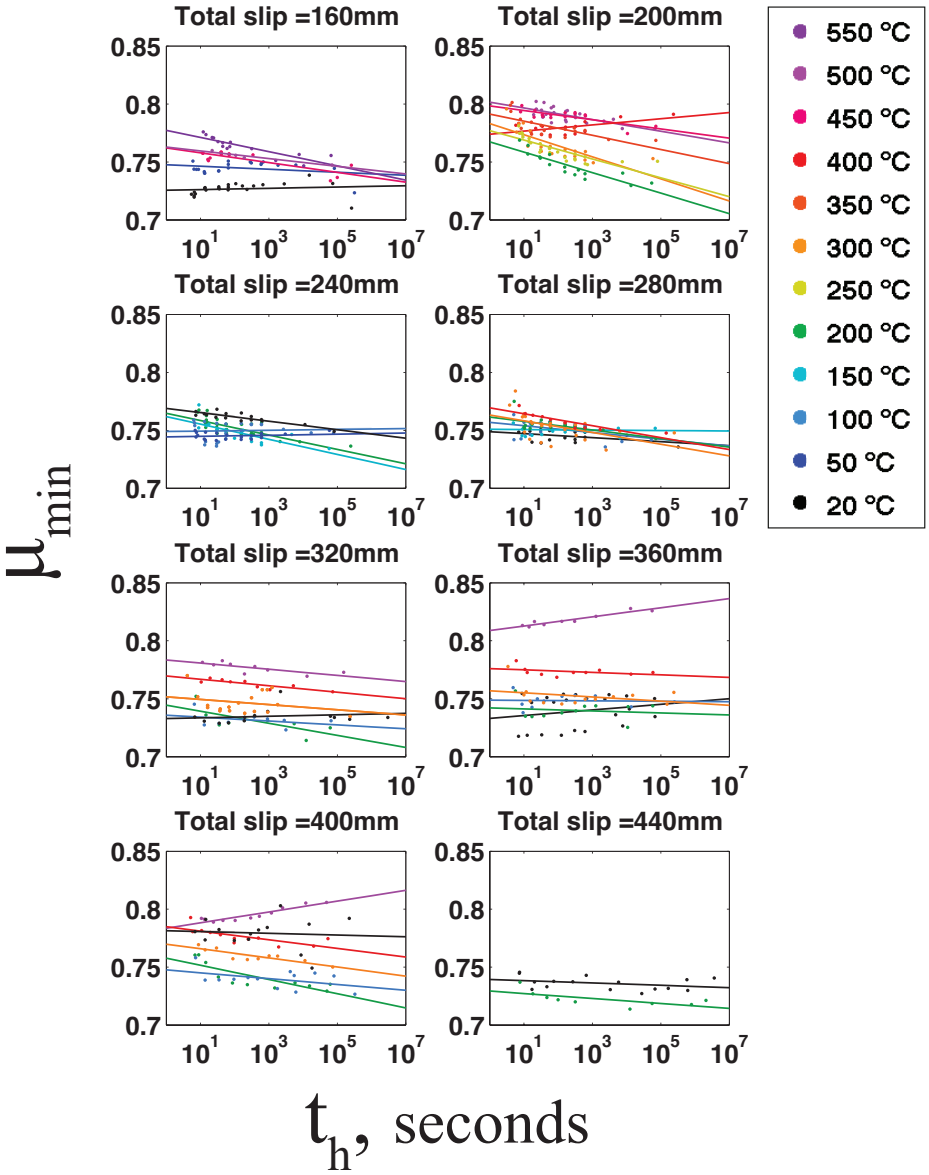

Figure S6. Minimum value of coefficient of friction reached right after rapid slip vs. hold time.

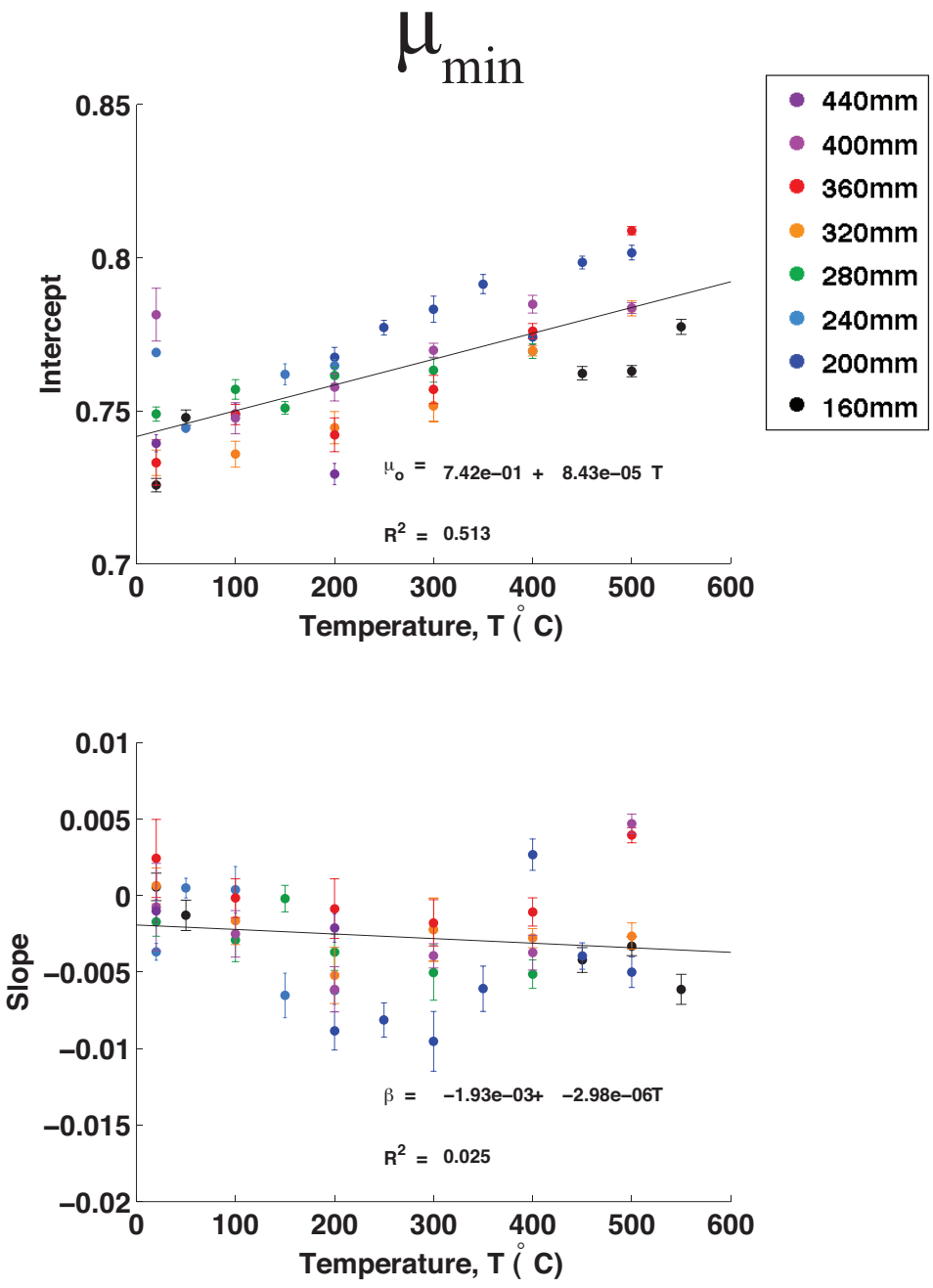

Figure S7. Slopes and intercepts fit to the μ_{min} data vs. temperature.

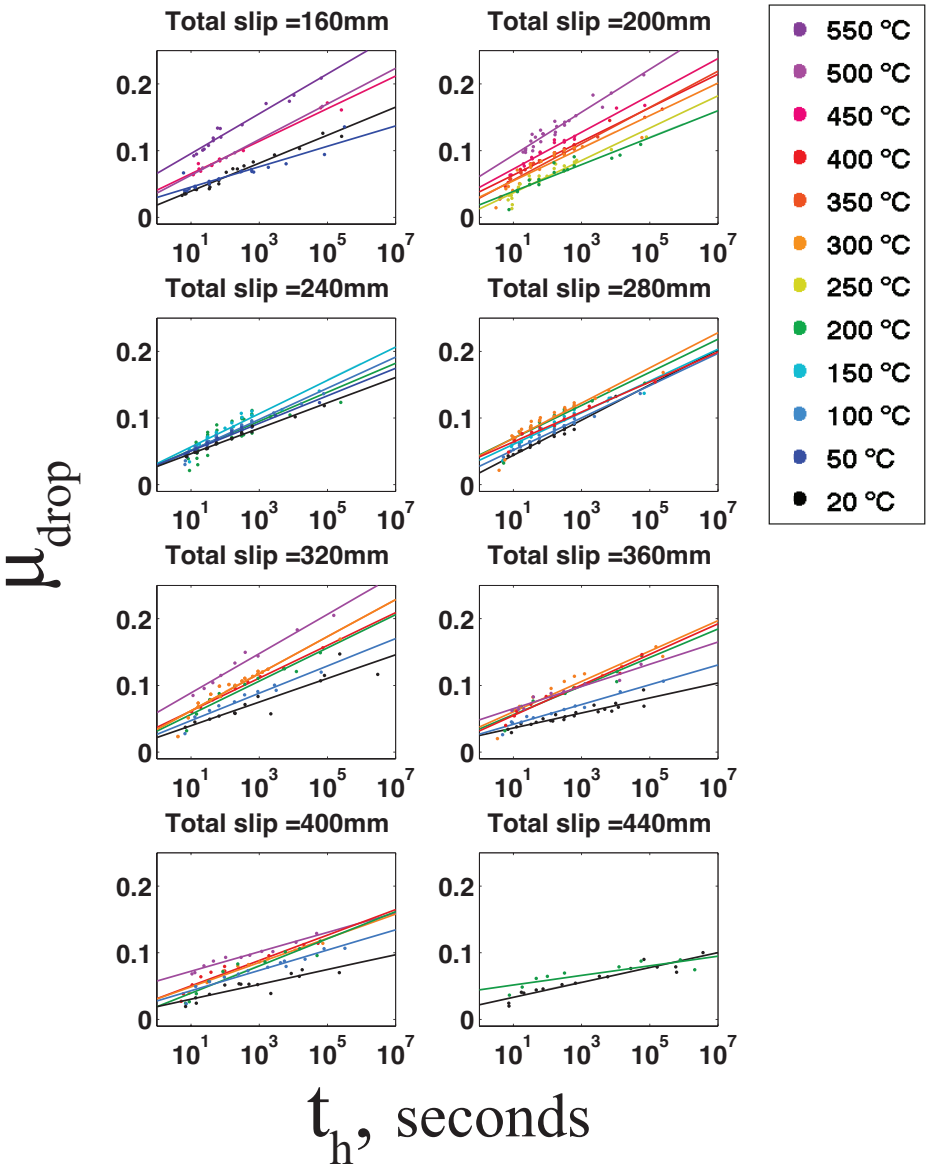

Figure S8. Drop in coefficient of friction during rapid slip from μ_s to μ_{min}.

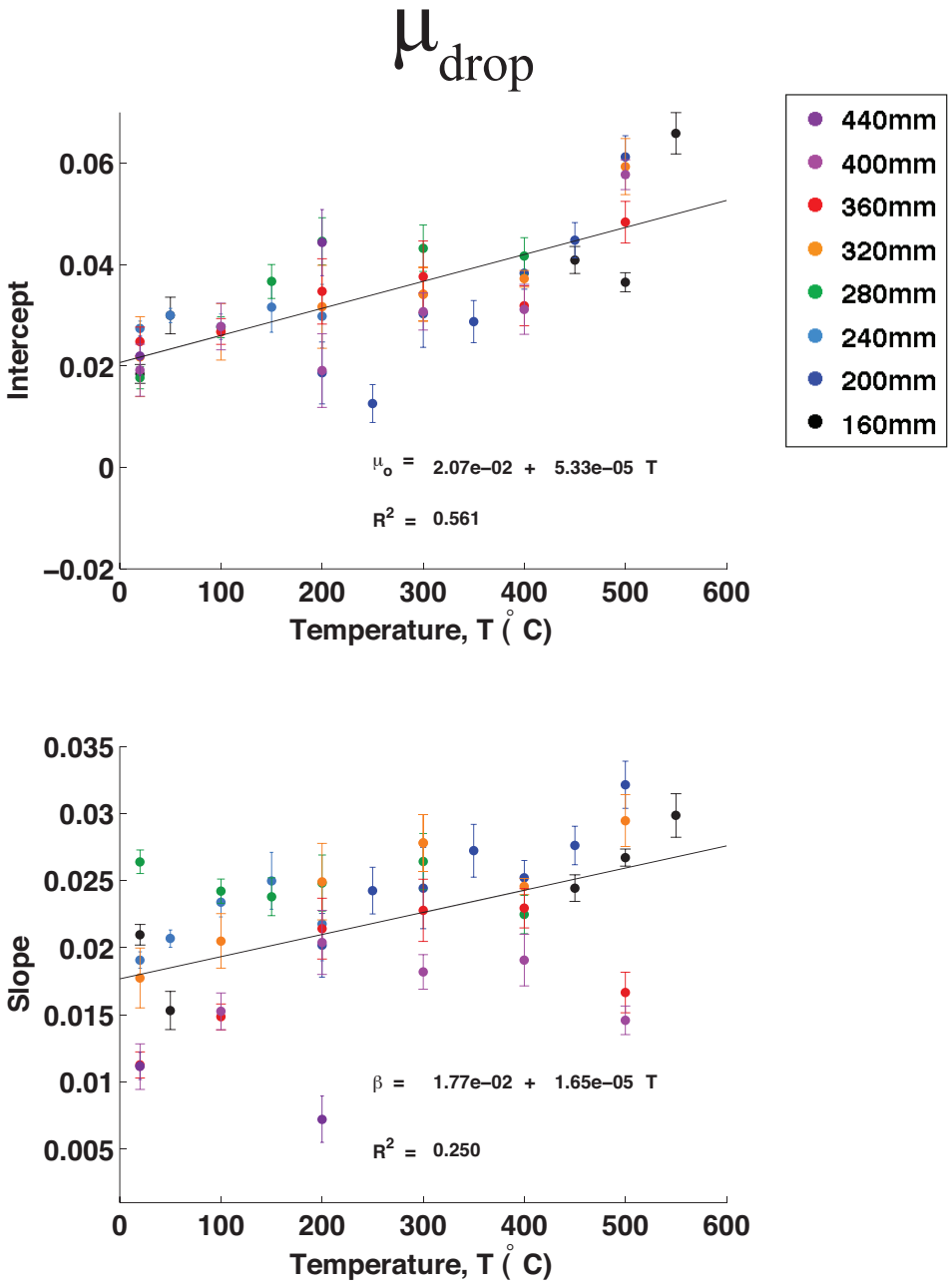

Figure S9. Slopes and intercepts fit to the μ_{drop} data vs. temperature.

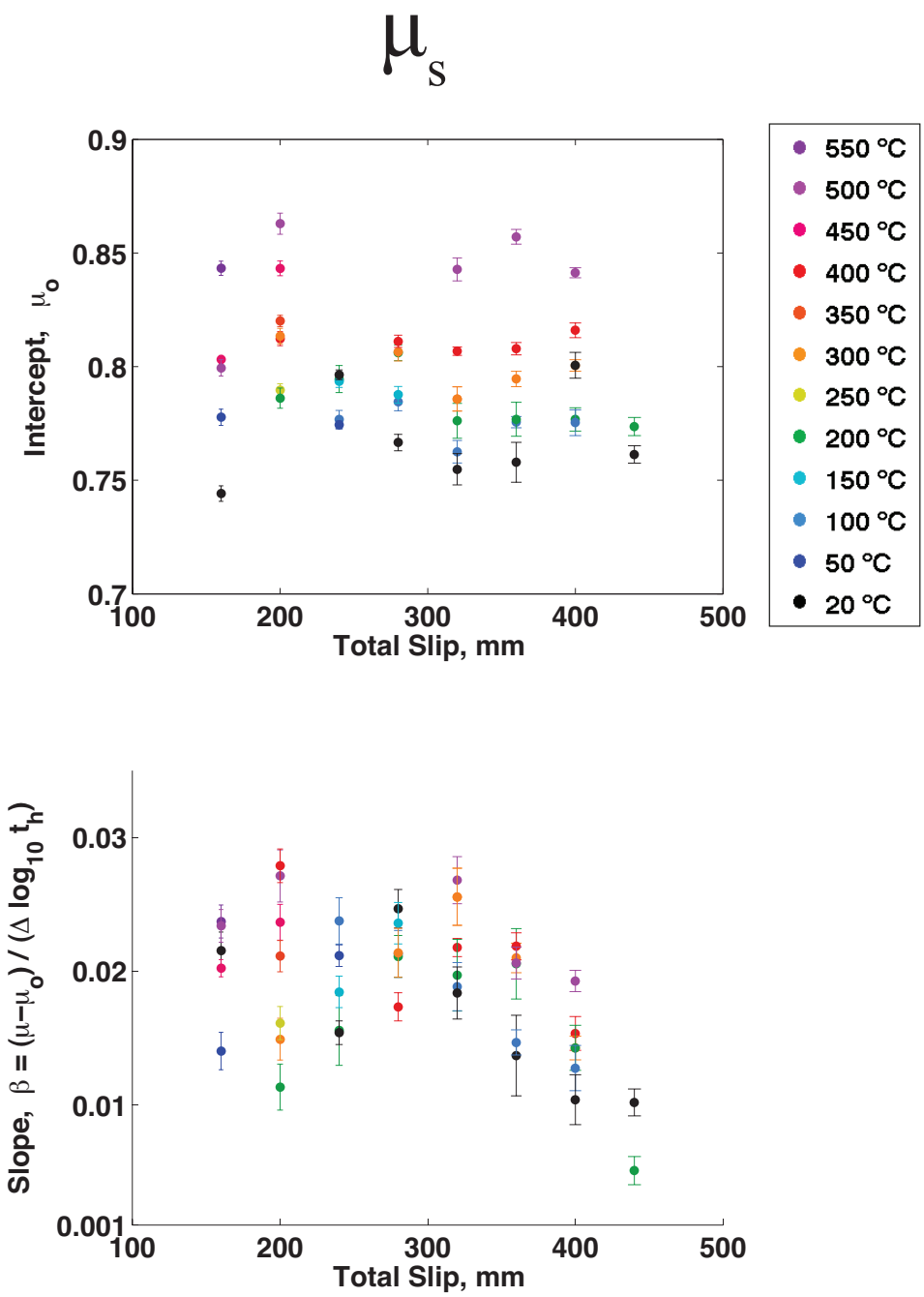

Figure S10. Slopes and intercepts fit to the μ_s data vs. total slip. Color represents temperature. Intercept is independent of total slip. Slope is mostly independent of total slip, except for a slight decrease in slope beyond 350 mm total slip.

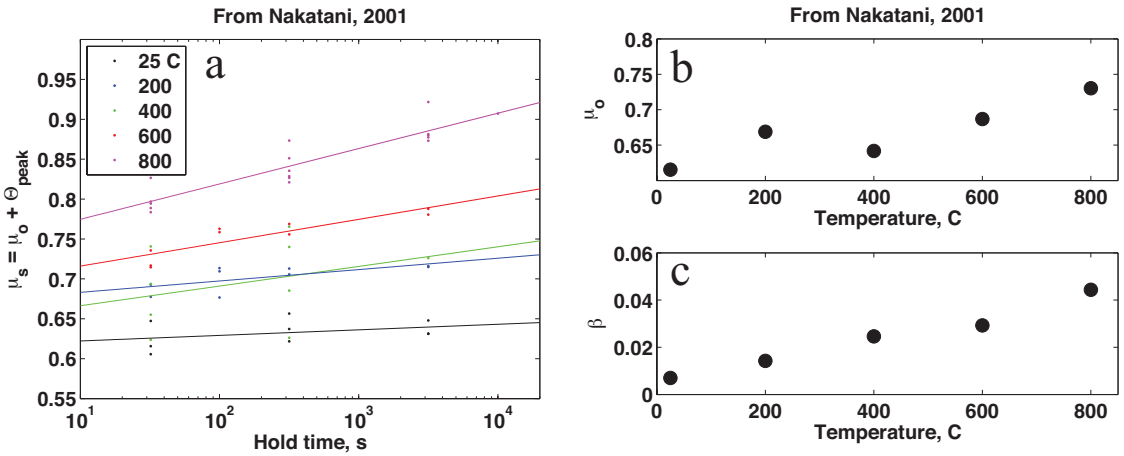

Figure S11. Data from Table 1 of (Nakatani, 2001). Their study was done at conditions similar to those of our experiments. They used a double direct shear apparatus to shear feldspar powder at 20 MPa normal stress and at temperature from 25 °C to 800 °C, under dry conditions. We interpret $\mu_s = \mu_* + \Theta$. (a) μ_s vs. hold time, where color represents temperature. (b) Intercept, μ_o, vs. temperature. (c) Slope, β, vs. temperature. Our results are in general agreement with those of Nakatani, except our values for μ_o are a little lower at all temperatures, and our value for β is a little higher at low temperature.

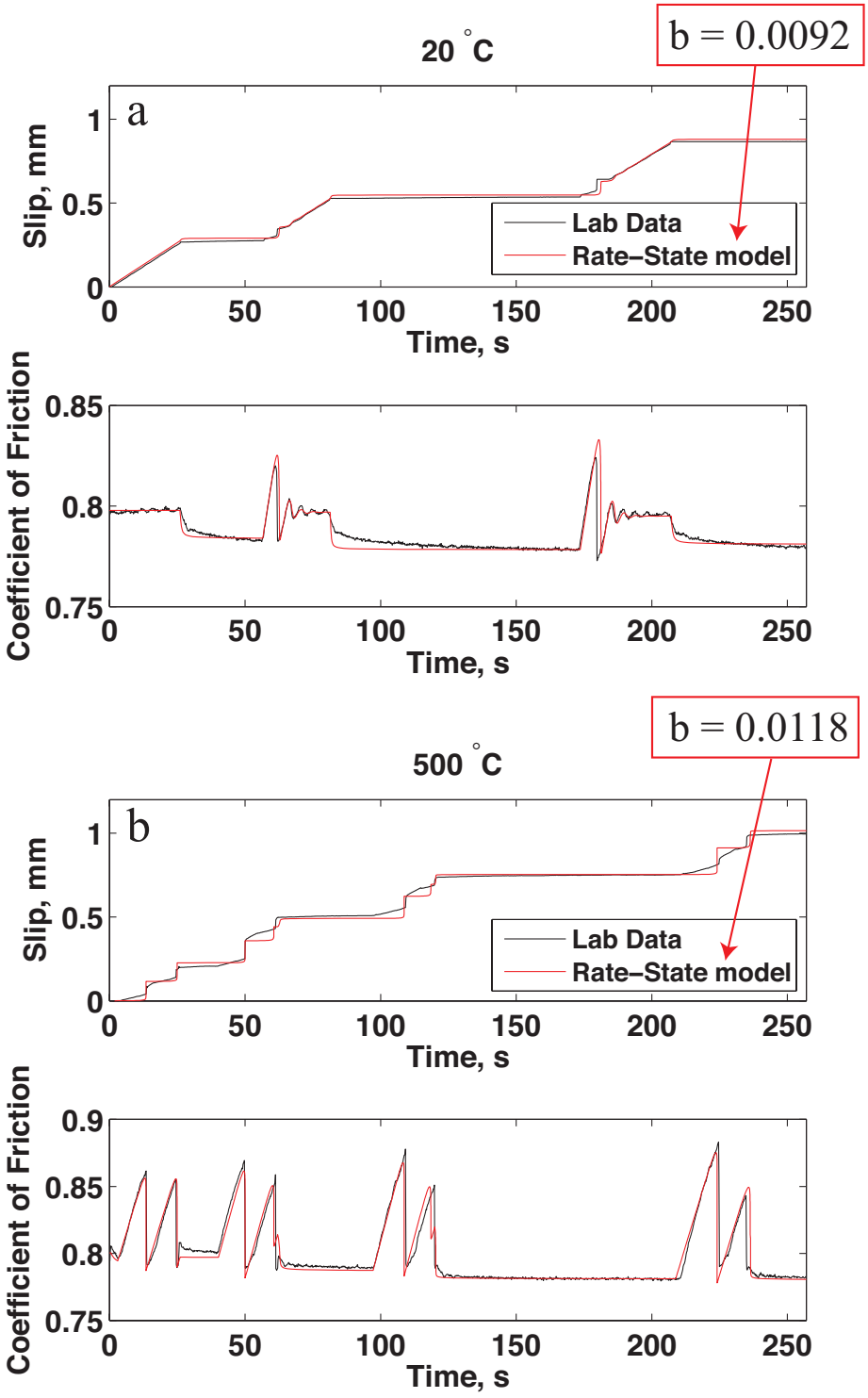

Figure S12. (a) Timeseries of slip and coefficient of friction at 20 °C, with laboratory data shownin black and the rate-state model shown in red. The model uses the rate-state parameter b equal to 0.0092, which is the value of b measured at room temperature from hold tests using $b = \Delta\mu_s / \Delta \ln t_h$. (b) Timeseries of slip and coefficient of friction at 500 °C, with laboratory data shown in black and the rate-state model shown in red. The model uses the rate-state parameter b equal to 0.0118, which is the value of b measured at 500 °C from hold tests using $b = \Delta\mu_s / \Delta \ln t_h$.

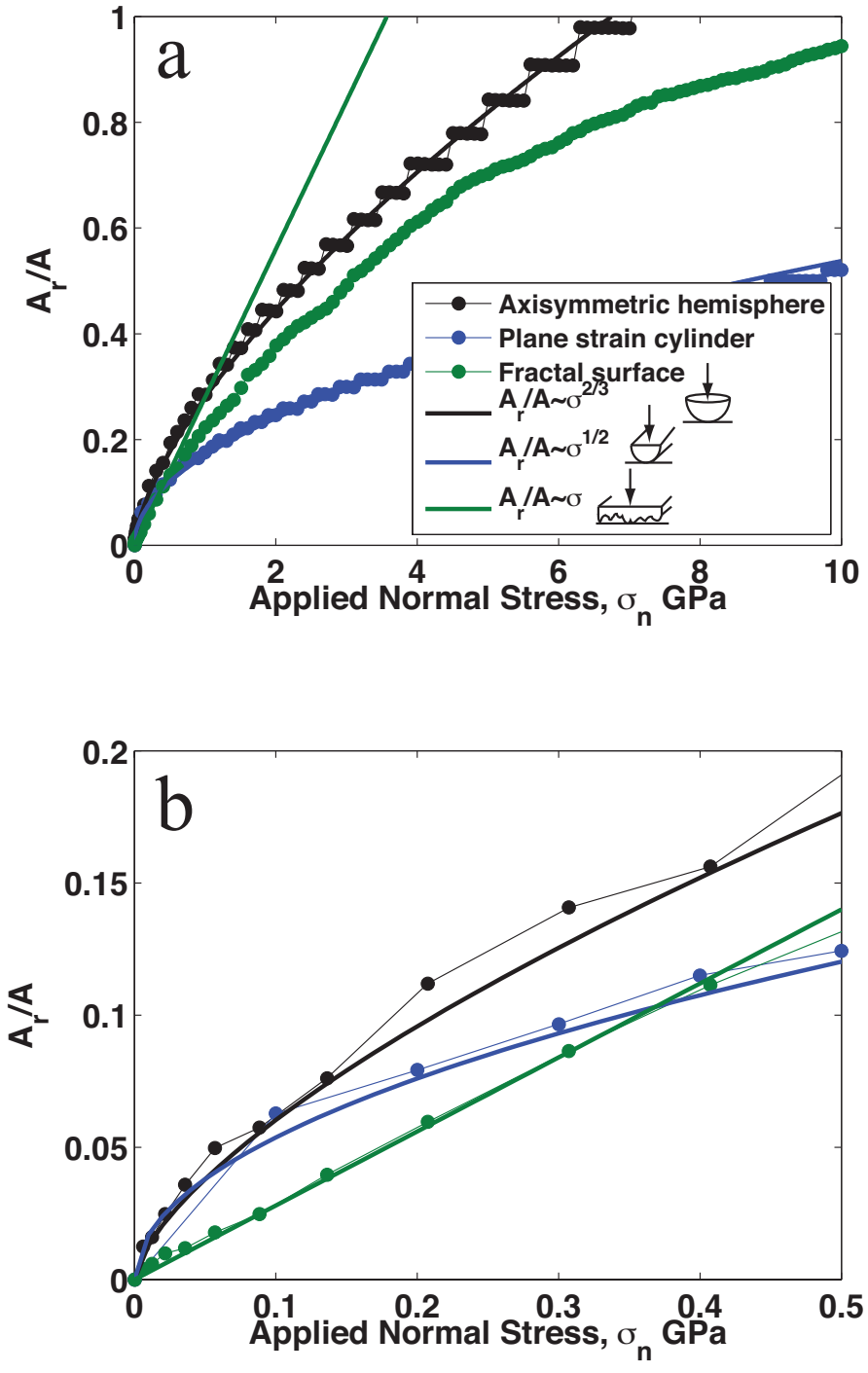

Figure S13. (a) Results of real contact area divided by total contact area, A_r/A, vs. applied normal stress, σ_n, from numerical models with different geometries and elastic rheology. Black dots are from a hemisphere, blue from a cylinder, and green from a fractal surface. Thick lines represent various stress- real contact area relationships. (b) Same as (a), but zoomed in to 0.5 GPa. The full numerical simulations in this study were performed at a normal stress of 0.05 GPa. Note that only the fractal surface produces a linear relationship between real contact area and applied normal stress. At very high applied normal stress the contact area becomes saturated, and the linear relationship does not hold.

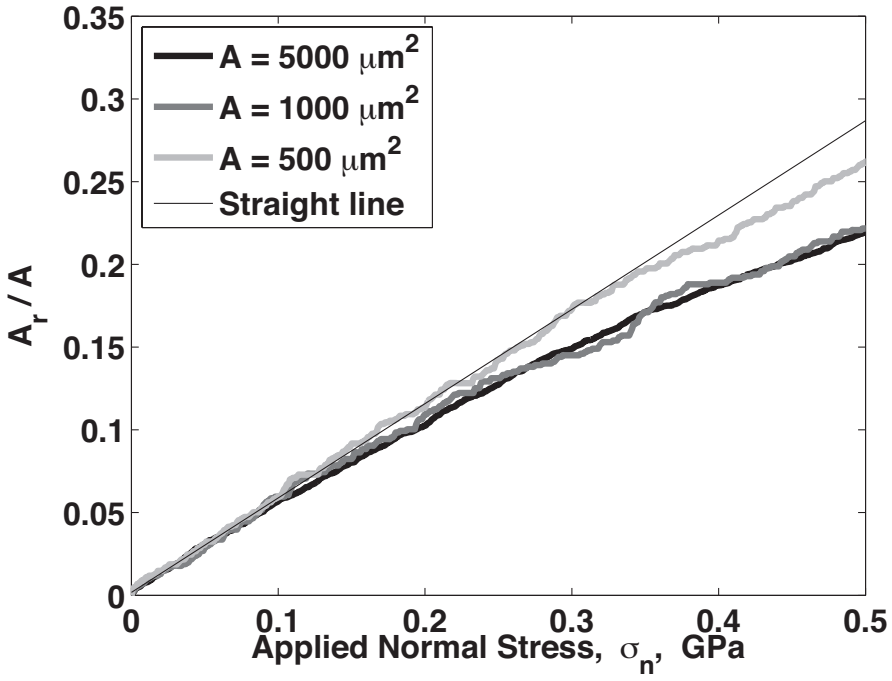

Figure S14. Ratio of real to total contact area as a function of normal stress for an elastic fractal sample pressed against a rigid flat surface. The black curve represents a 5000 μm long surface, the gray curve represents a 1000 μm long surface, and the light gray curve represents a 500 μm long surface. The thin black line is a straight line for reference. Note that up to about 0.1-0.2 GPa the curves are coincident (verification of Amonton's first law) and essentially straight (verification of Amonton's second law).

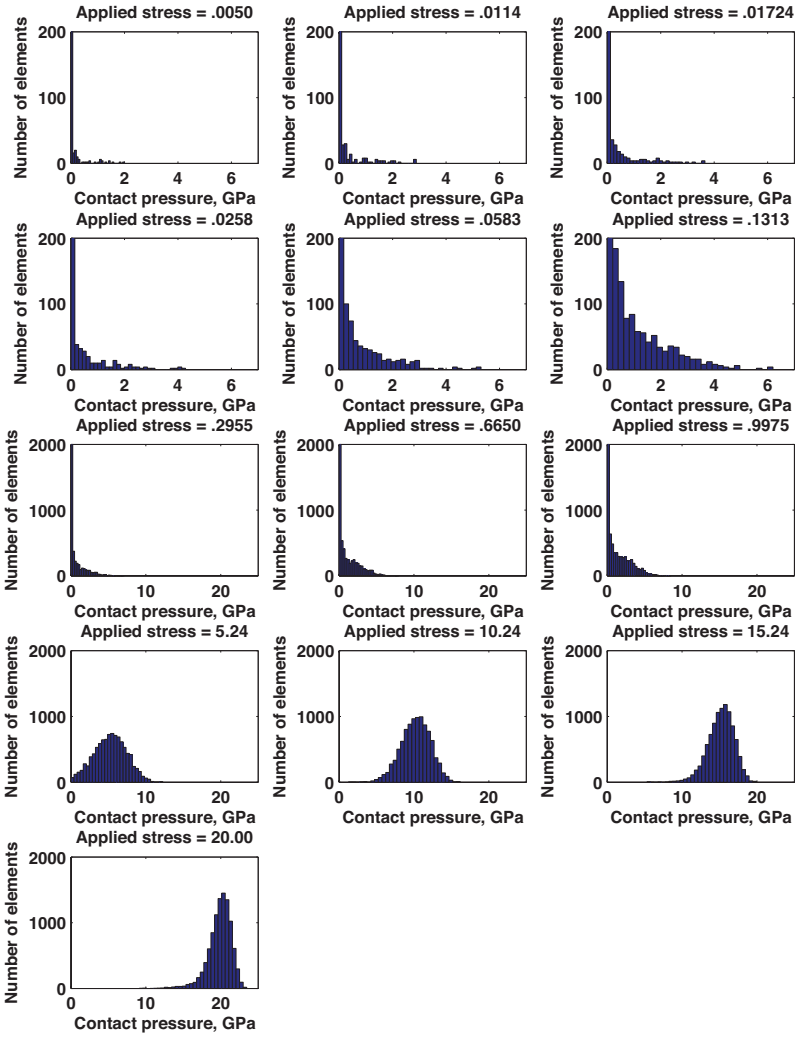

Figure S15. Distribution of normal stress at contacting regions (contact pressure) between the fractal surface and the rigid flat surface for a range of applied normal stresses. In the first two rows, the maximum number of elements has been capped at 200, to see more detail at higher contact pressures. The sample has an elastic rheology. At the lowest applied normal stresses, the maximum contact pressure reached is relatively high because the real contact area is very small. As applied stress is increased, the real contact area increases, with little effect on the maximum contact pressure. This relationship holds in the range of applied stresses used in rock friction laboratory experiments. Once the real contact area starts to become saturated $A_r/A \sim 1$, the geometry is less like a fractal and more like a rectangle, and the distribution of contact pressure centers around the applied stress. Behavior of the model in this regime is inconsistent with the adhesion theory.